



Syntheses, crystal structures, thermodynamic and fluorescent properties of dinuclear lanthanide complexes constructed with 2-fluorobenzoic acid and 5,5'-dimethyl-2,2'-bipyridine

Dan-Dan Du^{1,2} · Ning Ren³ · Jian-Jun Zhang^{1,2}

Received: 5 August 2020 / Accepted: 8 January 2021 / Published online: 6 February 2021
© Akadémiai Kiadó, Budapest, Hungary 2021

Abstract

2-fluorobenzoic acid and 5,5'-dimethyl-2,2'-bipyridine were used to construct two novel isostructural lanthanide complexes $[\text{Ln}(2\text{-FBA})_3(5,5'\text{-DM-2,2'-bipy})]_2$ (Ln = Eu(1), Tb(2); 2-FBA = 2-fluorobenzoate; 5,5'-DM-2,2'-bipy = 5,5'-dimethyl-2,2'-bipyridine) by conventional solution method. They were characterized by infrared spectroscopy (IR), elemental analysis and single-crystal X-ray diffraction. The crystal description based on single-crystal X-ray diffraction data revealed that both of the complexes gave the triclinic crystal structure, belonging to the $P\bar{1}$ space group. The two complexes were an infinite one-dimensional (1D) chain by hydrogen bonding (C–H \cdots F) interactions to give a 2D supermolecular structure. Additionally, thermal behavior of the complexes was investigated by TG-DSC/FTIR technology in detail. The molar heat capacities of the two complexes in the temperature range of 278.15–423.15 K were determined by a DSC instrument, and their thermodynamic functions ($H_T - H_{298.15\text{ K}}$) and ($S_T - S_{298.15\text{ K}}$) were calculated. Beyond that, the fluorescence spectra and fluorescence lifetime of the complexes 1 and 2 were also evaluated.

Keywords Lanthanide complexes · X-ray structure · 2-fluorobenzoic acid · TG-DSC/FTIR · Heat capacity · Fluorescence

Introduction

In recent years, the structures and properties of lanthanide complexes have been the focus of attention. This is mainly due to its superior functional properties and extensive applications in magnetic materials [1, 2], catalysts [3–5], luminescent materials [6, 7], biology [8–10] and so on. In particular, trivalent lanthanide ions have become attractive light sources due to their excellent luminescent purity and

long excited state lifetime [11]. For instance, Eu(III) and Tb(III) complexes have evoked considerable attention since they emit strong red or green luminescence under ultraviolet light, respectively [12]. However, the f-f electron transition between configurations is forbidden, which makes it difficult for lanthanide ions to directly absorb light [13, 14]. In order to make up for this deficiency, the introduction of organic ligands plays an important role in improving the emission efficiency of lanthanides. The reason why the absorbed energy can be effectively transferred to the central lanthanide ions is that they greatly enhance the absorption of light [15, 16]. This process, created by Weissman, is later called the antenna effect [17]. On the other hand, due to the unique structure of 4f electrons, Ln(III) ions have a high affinity for hard donor atoms such as carboxyl oxygen atoms, and the ligands containing carboxyl groups have various coordination modes [18], including single-tooth, double-tooth chelation, bridging three teeth, bridging four teeth, etc. Apart from that, the addition of auxiliary organic ligands such as 5,5'-dimethyl-2,2'-bipyridine not only saturates the coordination of lanthanide ions but also allows the lanthanide complexes to have higher thermal stability and stronger luminescence [19].

Supplementary information The online version of this article (<https://doi.org/10.1007/s10973-021-10563-2>)

✉ Ning Ren

✉ Jian-Jun Zhang
jjzhang6@126.com

- ¹ Testing and Analysis Center, Hebei Normal University, Shijiazhuang 050024, P. R. China
- ² College of Chemistry & Material Science, Hebei Normal University, Shijiazhuang 050024, P. R. China
- ³ College of Chemical Engineering & Material, Hebei Key Laboratory of Heterocyclic Compounds, Handan University, Handan 056005, P. R. China

In recent years, the thermodynamic properties of complexes, such as kinetic mechanism of thermal decomposition and heat capacity, have been crucial in estimating thermal stability and heat release [20–23]. Among them, the heat capacity is an important thermophysical quality, which not only provides a good theoretical basis for the study of thermodynamics, but also plays an important role in the design of chemical processes [24]. The heat capacity value can be determined using numerous methods with different calorimetry instruments, of which the differential scanning calorimeter (DSC) is one of the most important research methods [25]. Many results, the DSC can provide molar heat capacities over the wide temperature range, enthalpy, entropy and Gibbs free energy can be received [26]. Consequently, heat capacity has very significant guiding role in the theoretical research and application development of the complexes.

Two lanthanide carboxylic acid complexes $[\text{Ln}(2\text{-FBA})_3(5,5'\text{-DM-2,2'-bipy})_2]$ ($\text{Ln} = \text{Eu}$ (1), Tb (2)) are successfully synthesized by a mixed ligand synthesis strategy of 2-fluorobenzoic acid (2-FBA) and 5,5'-dimethyl-2,2'-bipyridine (5,5'-DM-2,2'-bipy). The crystal structures of the two complexes are determined by single-crystal X-ray diffraction. And they are characterized using elemental analysis and IR. Simultaneously, TG-DSC/FTIR is used to analyze the thermal decomposition of the two complexes, and the heat capacities of the two complexes are determined by differential scanning calorimetry method. The luminescence studies indicate that complexes 1 and 2 exhibit fluorescence centered on lanthanide ions.

Experimental

Chemicals and materials

The $\text{Ln}(\text{NO}_3)_3 \cdot 6\text{H}_2\text{O}$, 2-FBA and 5,5'-DM-2,2'-bipy are all purchased from Beijing Innochem Science & Technology Co., Ltd, and can be used directly without further treatment.

Characterizations

X-ray diffraction data are obtained on the Bruker AXS single-crystal diffractometer with $\text{Mo-K}\alpha$ (0.71073 Å) and $\text{Cu-K}\alpha$ (1.54178 Å) rays monochromized by graphite as the incident light source. The structures are analyzed by direct methods and refined on F^2 by full-matrix least-square method in SHELXS-97 program package. An elemental analysis apparatus (Elemental vario EL cube) is used to analyze the C, H, N of the complexes and the metal content is obtained by complexometric titration with standard EDTA solution. The IR analysis is recorded as KBr pellets using a Bruker TENSOR 27 spectrometer, which spans from 4000 to 400 cm^{-1} .

A NETASCH STA 449 F3 instrument with a Bruker TENSOR 27 Fourier analyzer is used to conduct thermal analysis and the three-dimensional infrared (FTIR) with a continuous heating rate of 10 $\text{K}\cdot\text{min}^{-1}$ under a simulated air atmosphere.

Over the temperature range from 278.15 to 423.15 K, the heat capacities of the complexes are measured in dynamic nitrogen atmosphere by indirect method with a linear heating rate of 10 $\text{K}\cdot\text{min}^{-1}$. Before determining the heat capacities of the complexes, the temperature and sensitivity of the instrument are adjusted by measuring the melting points of six standard solutions. The heat capacities of reference standards, namely sapphire and $\alpha\text{-Al}_2\text{O}_3$, are determined simultaneously. The result shows that the relative deviation between our calibration data and the NIST recommended values is less than 0.3%. Fluorescence spectra and fluorescence lifetime are measured with an Edinburgh instruments FS5 spectrofluorophotometer.

Synthesis

2-FBA (0.6 mmol) and 5,5'-DM-2,2'-bipy (0.2 mmol) were dissolved in 7 mL 95% ethanol. Slowly add 1.0 mol L^{-1} NaOH solution, carefully adjust the pH value of reaction mixture to about 5–6, and then add 3.5 mL $\text{Ln}(\text{NO}_3)_3 \cdot 6\text{H}_2\text{O}$ aqueous solution. Stir continuously for 7 h, then let stand for 12 h. Finally, the mother liquor can be collected through filtration, and the ideal crystals can be obtained after one week at room temperature. Anal. Calc. for $\text{C}_{66}\text{H}_{48}\text{Eu}_2\text{F}_6\text{N}_4\text{O}_{12}$ (%): C, 52.60; H, 3.21; N, 3.72; Eu, 20.17. Found: C, 52.54; H, 3.21; N, 3.61; Eu, 19.75. Anal. Calc. for $\text{C}_{66}\text{H}_{48}\text{F}_6\text{N}_4\text{O}_{12}\text{Tb}_2$ (%): C, 52.23; H, 3.19; N, 3.69; Tb, 20.90. Found: C, 52.20; H, 3.16; N, 3.65; Tb, 20.87.

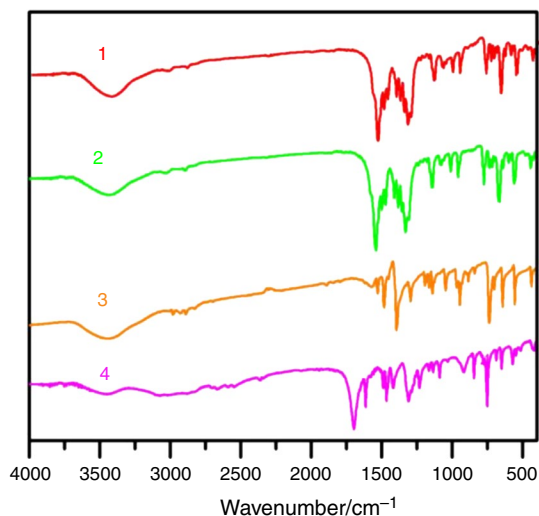
Results and discussion

Infrared spectroscopy

IR spectra of the two complexes and ligands have been recorded in the region of 4000–400 cm^{-1} . From the results, two complexes have similar spectra, indicating that they have the same configuration [27]. Here, only complex 1 is used as an example for analysis. The important infrared data of ligands and prepared complexes at characteristic frequencies are listed in Table 1. In ligand 2-FBA, a strong absorption band is found at 1697 cm^{-1} , which is assigned to the stretching frequency of the carboxylate group ($\nu_{\text{C=O}}$) (Fig. 1). For complex 1, antisymmetric $\nu_{\text{as}(\text{COO}^-)}$ and symmetric $\nu_{\text{s}(\text{COO}^-)}$ stretching vibrations appear at 1569 and 1430 cm^{-1} , respectively. Another new absorption peak in the complex appears at 416 cm^{-1} is attributed to the formation of Ln–O bond. All these changes indicate that the oxygen

Table 1 IR bands of ligands and their lanthanide complexes (values in cm^{-1})

Ligands/complexes	$\nu_{\text{C}=\text{N}}$	$\delta_{\text{C}-\text{H}}$	$\nu_{\text{C}=\text{O}}$	$\nu_{\text{as}}(\text{COO}^-)$	$\nu_{\text{s}}(\text{COO}^-)$	$\nu_{(\text{Ln}-\text{O})}$
5,5'-DM-2,2'-bipy	1467	827	736	–	–	–
2-FBA	–	–	–	1697	–	–
1	1457	810	679	–	1569	1430
2	1458	811	679	–	1570	1432

**Fig. 1** IR spectra of complex 1 (1), complex 2 (2), 5,5'-DM-2,2'-bipy (3), 2-FBA (4)

atoms of the carboxylate groups are engaged in the bond with the central metal ions [28]. In addition to the above characteristic bands, the characteristic absorption peak of 5,5'-DM-2,2'-bipy, C=N (1467 cm^{-1}), is blue-shifted to 1457 cm^{-1} , indicating that the nitrogen atoms have been coordinated with the central Eu(III) ions [29].

Crystal structural descriptions

A summary of the complexes crystallographic data and structure refinement are provided in Table 2. Selected major bond lengths (\AA) in the structures of 1–2 are shown in Table 3. The single-crystal X-ray crystallography indicates that 1–2 are isostructural complexes with dinuclear structures, crystallizing in $P\bar{1}$ space group of the triclinic system. Hereby the structure of complex 1 is selected as a representative example for detailed description.

As displayed in Fig. 2a, the molecular structure of $[\text{Eu}(\text{2-FBA})_3(\text{5,5'-DM-2,2'-bipy})]_2$ is composed of two Eu(III) ions, six 2-FBA ligands and two 5,5'-DM-2,2'-bipy neutral ligands. The coordination number of Eu(III) is 9. In this coordination sphere, three of the seven oxygens are from two bridging tridentate 2-FBA ligands (O1#, O1 and O2), two oxygen atoms (O3 and O4) originate from two bridging bidentate carboxylate groups of 2-FBA ligands, the rest

are the chelating bidentate group of 2-FBA ligand (O5 and O6), and the chelating bidentate ligand 5,5'-DM-2,2'-bipy provides two N1 and N2 atoms, forming a distorted triangular prism configuration (Fig. 2b). Additionally, the length of Eu–O bond is 2.370–2.623 \AA , with an average of 2.455 \AA ; and the important bond lengths of Eu–N bonds are 2.588 and 2.660 \AA , with an average of 2.624 \AA , which are consistent with previous studies [30]. It should be noted that the Eu–N bond is slightly longer than the Eu–O bond, which may be due to the fact that lanthanide metals are easier to coordinate with oxygen atoms.

As shown in Fig. 3a, two adjacent 2-FBA ligands pass through weak hydrogen bonds (C–H \cdots F) form a one-dimensional chain supramolecular structure along the a-axis direction. We also note that the weak hydrogen bond distance between the fluorine atom of bridging tridentate 2-FBA and the carbon atom of bridging bidentate 2-FBA is 3.222 \AA . Interestingly, these 1D chains are connected by the weak hydrogen bond interaction between 2-FBA ligand and 5,5'-DM-2,2'-bipy with the C–H \cdots F distance of 3.556 \AA , thereby generating a 2D network (Fig. 3b).

At 2018, Zhu Min-Min et al. have reported the complex $[\text{Eu}(\text{3,4-DMBA})_3(\text{3,4-DMHBA})(\text{5,5'-DM-2,2'-bipy})]_2$ [31]. The complex is binuclear, each Eu(III) ion is nine-coordinated with a distorted monocapped square antiprismatic coordination geometry. Moreover, the structure also contains two nonprotonated 3,4-DMHBA ligands. The main ligand 3,4-DMBA adopts three coordination modes with the Eu(III) centers: monodentate, bridging bidentate and bridging tridentate. While the complex 1 $[\text{Eu}(\text{2-FBA})_3(\text{5,5'-DM-2,2'-bipy})]_2$ is binuclear and each Eu(III) is nine-coordinated with a distorted triangular prism configuration. The 2-FBA ligand adopts three coordination modes: bidentate bridging chelating bidentate and bridging tridentate. The thermal stability of the complexes is also affected by the structures. Because $[\text{Eu}(\text{3,4-DMBA})_3(\text{3,4-DMHBA})(\text{5,5'-DM-2,2'-bipy})]_2$ begins to decompose at 317.15 K, while the molecular structure of complex 1 begins to decompose at 462.15 K. Not only that, the fluorescence property of complex 1 is stronger than that of complex $[\text{Eu}(\text{3,4-DMBA})_3(\text{3,4-DMHBA})(\text{5,5'-DM-2,2'-bipy})]_2$, according to the experimental results of fluorescence lifetime. At 2019, Li Ying-Ying et al. have reported the complex $[\text{Tb}(\text{2,3-DMOBA})_3(\text{5,5'-DM-2,2'-bipy})]_2 \cdot \text{C}_2\text{H}_5\text{OH}$ [32]. The complex is binuclear and each Tb(III) ion is nine-coordinated

Table 2 Single-crystal data and refinement details for complexes 1–2

Complexes	1	2
Formula	C ₆₆ H ₄₈ Eu ₂ F ₆ N ₄ O ₁₂	C ₆₆ H ₄₈ F ₆ Tb ₂ N ₄ O ₁₂
Formula weight/g mol ⁻¹	1507.00	1520.92
T/K	298(2)	298(2)
Wavelength/Å	0.71073	0.71073
Crystal system	Triclinic	Triclinic
Space group	<i>P</i> $\bar{1}$	<i>P</i> $\bar{1}$
<i>a</i> /Å	11.2590(11)	11.2301(12)
<i>b</i> /Å	12.1769(12)	12.0848(11)
<i>c</i> /Å	12.8701(13)	12.7843(14)
α /°	103.511(3)	103.213(2)
β /°	114.032(4)	114.301(4)
γ /°	99.102 (2)	99.1840(1)
Volume/Å ³	1501.8(3)	1475.2(3)
<i>Z</i> , calculated density/Mg m ⁻³	1, 1.666	1, 1.712
Absorption coefficient/mm ⁻¹	2.155	2.465
<i>F</i> ₀₀₀	748	752
Crystal size/mm ³	0.40×0.27×0.15	0.37×0.20×0.16
θ range for data collection/°	2.70 to 25.02	2.72 to 25.02
Limiting indices	-13 ≤ <i>h</i> ≤ 8 -12 ≤ <i>k</i> ≤ 14 -14 ≤ <i>l</i> ≤ 15	-7 ≤ <i>h</i> ≤ 13 -14 ≤ <i>k</i> ≤ 14 -15 ≤ <i>l</i> ≤ 15
Reflections collected/unique	7685/5224 [<i>R</i> _(int) = 0.0268]	7576/5130 [<i>R</i> _(int) = 0.0405]
Completeness to $\theta = 25.02^\circ$	98.3%	98.4%
Max. and min. transmission	0.7381 and 0.4794	0.6938 and 0.4624
Data/restraints/parameters	5224/187/432	5130/168/425
Goodness-of-fit on <i>F</i> ²	1.020	1.021
<i>R</i> ₁	0.0361	0.0406
w <i>R</i> ₂	0.0877	0.1035
<i>R</i> ₁ (all data)	0.0446	0.0491
w <i>R</i> ₂ (all data)	0.0936	0.1111
Largest diff. peak and hole/(e ⁻ ·Å ⁻³)	1.567 and -0.622	1.742 and -1.152

Table 3 The main bond lengths (Å) for complexes 1 and 2

Complex 1	Bond length/Å	Complex 2	Bond length/Å
Eu(1)-O(4)#1	2.370(3)	Tb(1)-O(2)#1	2.330(3)
Eu(1)-O(1)	2.377(3)	Tb(1)-O(3)	2.343(3)
Eu(1)-O(3)	2.390(3)	Tb(1)-O(1)	2.356(4)
Eu(1)-O(5)	2.438(3)	Tb(1)-O(6)	2.401(4)
Eu(1)-O(6)	2.487(3)	Tb(1)-O(5)	2.457(4)
Eu(1)-O(2)#1	2.503(3)	Tb(1)-O(4)#1	2.462(4)
Eu(1)-N(2)	2.588(4)	Tb(1)-N(2)	2.546(4)
Eu(1)-O(1)#1	2.623(3)	Tb(1)-O(3)#1	2.597(4)
Eu(1)-N(1)	2.660(4)	Tb(1)-N(1)	2.619(4)

with a distorted monocapped square antiprismatic coordination geometry. The 2,3-DMOBA ligand adopts three coordination modes: bidentate bridging, chelating bidentate and

bridging tridentate. Among them, the reason the complex [Tb(2,3-DMOBA)₃(5,5'-DM-2,2'-bipy)]₂·C₂H₅OH begins to decompose at 354.15 K is that it contains a free ethanol molecule. And the luminescent lifetime of the complex is reported to be 1.175 ms. By comparison, we find that these acidic ligands generate a specific base for the formation of the whole structure, which may be due to the difference in substituents and steric hindrance in the carboxylic acid ligands. Therefore, the thermal stability and fluorescence properties of the complexes are directly affected.

Thermal analysis

The thermal properties of luminescent materials, especially the stability and volatility, are of great significance for the practical application of luminescent materials. Hence, under the conditions of a simulated air atmosphere

Fig. 2 **a** The asymmetric unit of complex 1. **b** Coordination environment of the Eu(III) in complex 1

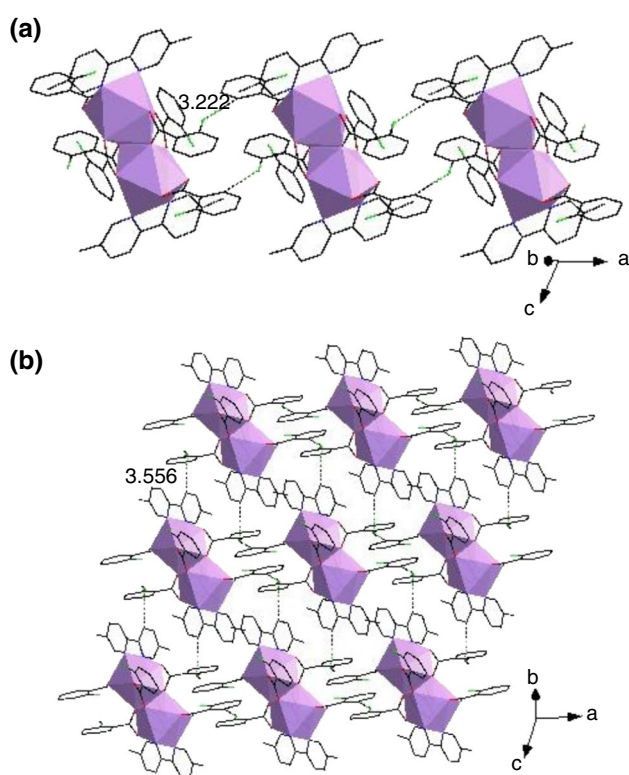
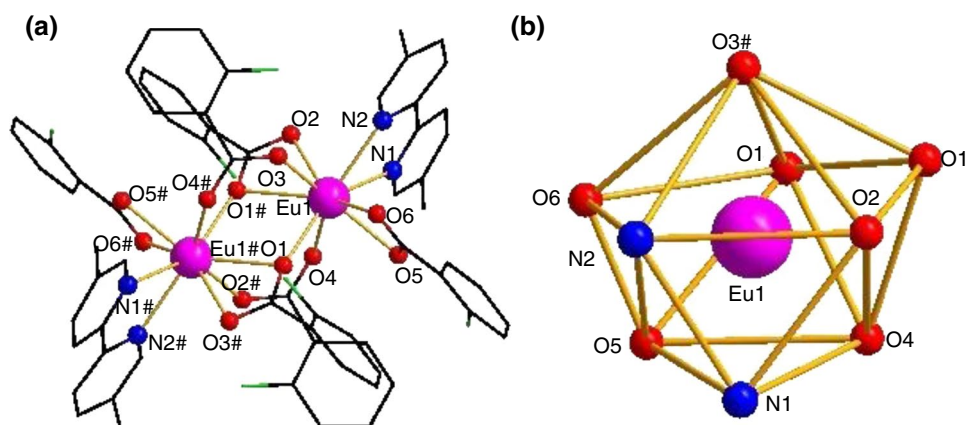


Fig. 3 **a** View of the 1D chain of complex 1 along the a axis. **b** 2D structure of complex 1 view from the ac direction

and the heating rate of $10 \text{ K} \cdot \text{min}^{-1}$, the TG-DTG-DSC curves of the complexes have been investigated in the temperature range of 300–1223.15 K (Fig. 4). The obtained thermal decomposition data are collected and tabulated in Table 4, and the three-dimensional infrared diagram of the gases escaping from complexes 1 and 2 is shown in Fig. 5. The strongest infrared absorption spectrum of escaping gas at different temperatures is presented in Fig. 6. Since the TG-DTG curve shows that the decomposition steps of the

two complexes are similar, complex 1 is as a representative of the detailed discussion.

The first mass loss of 24.36% (calculated = 24.25%) that occurs at 456.15–595.15 K, attributes to the loss of two 5,5'-DM-2,2'-bipy ligands. At this time, the DSC curve gives a small endothermic peak ($T = 536.75 \text{ K}$, $\Delta H = 135.2 \text{ J g}^{-1}$). The signal peak at 540.97 K is the strongest in the infrared spectrum of the corresponding escaping gas product. Among them, the characteristic absorption bands of H_2O ($3565\text{--}3745 \text{ cm}^{-1}$) and CO_2 ($2310\text{--}2388$, 654 cm^{-1}) are detected. Besides, the absorption peaks of some small organic molecule fragments are detected. For example, $\nu_{\text{C}=\text{N}}$ (1471 cm^{-1}), $\nu_{\text{C}-\text{N}}$ (1132 , 1216 cm^{-1}), $\nu_{\text{C}=\text{C}}$ (1558 , 1600 cm^{-1}), $\nu_{\text{C}-\text{H}}$ ($2933\text{--}3014 \text{ cm}^{-1}$), $\gamma_{\text{C}-\text{H}}$ (1060 , 1031 , 825 cm^{-1}). The second mass loss from 595.15 to 1216.55 K is 49.77%, which is consistent with the loss of all 2-FBA ligands (calculated = 52.20%). And an exothermic peak ($T = 740.75 \text{ K}$, $\Delta H = 3484 \text{ J g}^{-1}$) is observed on the DSC curve. Meanwhile, the absorption band of H_2O ($3587\text{--}3735 \text{ cm}^{-1}$) and the characteristic absorption peak of CO_2 ($2268\text{--}2391$, 669 cm^{-1}) are found in the infrared spectrum of $T = 741.70 \text{ K}$. Therefore, the remaining residue is Eu_2O_3 , with the total mass of 74.13%, which is in good agreement with the theoretical mass of 76.65%.

Heat capacities of complexes

When determining the molar heat capacities of the complexes, there is no thermal anomaly within the range of 278.15–423.15 K, indicating that the two complexes have stable thermodynamic properties. The average molar heat capacities data are listed in Tables S1 and S2 and plotted in Fig. 7. As seen in Fig. 7, the complexes have similar molar heat capacities, indicating that they have the same crystal structure. Furthermore, with the increase in temperature, the values of $C_{p,m}$ of the two complexes increase gradually, and the curves are smooth in the whole temperature segment, which means that there is no phase

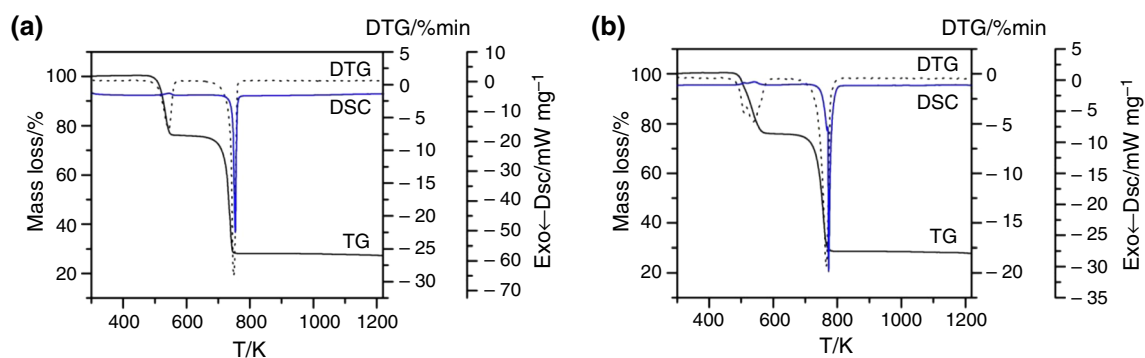
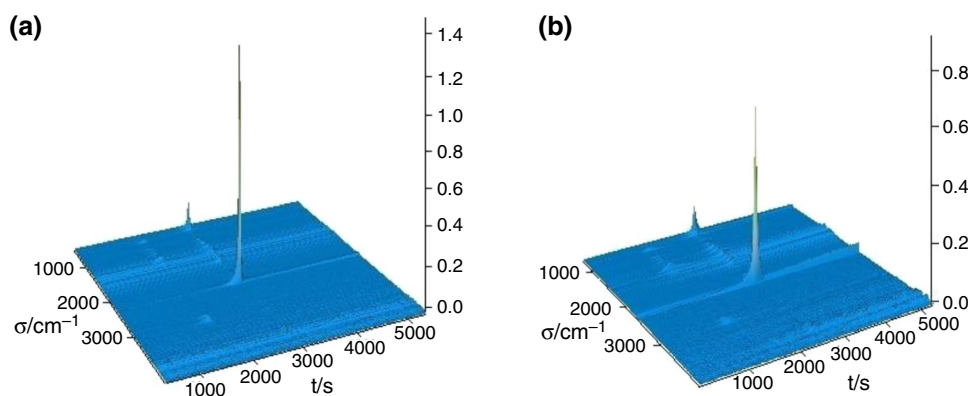


Fig. 4 TG-DTG-DSC curves of complexes 1 **a** and 2 **b** at a heating rate of 10 K·min⁻¹

Table 4 The thermodynamic data of the synthesized complexes

Complexes	Steps	Temperature range/K	DTG T _p /K	Mass loss rate/%		Probable expelled groups	Intermediate and residue
				Found	Calcd		
1	I	462.15–553.15	533.95	24.36	24.45	2(5,5'-DM-2,2'-bipy)	[Eu ₂ (2-FBA) ₆]
	II	553.15–1206.15	735.05	49.77	52.20	6(2-FBA)	Eu ₂ O ₃
				74.13	76.65		
2	I	458.15–581.15	532.95	24.53	24.23	2(5,5'-DM-2,2'-bipy)	[Tb ₂ (2-FBA) ₆]
	II	581.15–1216.55	755.35	48.06	51.19	6(2-FBA)	Tb ₄ O ₇
				72.59	75.42		

Fig. 5 Stacked plots of the evolved gases for complexes 1 **a** and 2 **b** as observed on an online TG-DSC/FTIR system



transition in this region. The polynomial equation of the two complexes can be obtained by fitting the experimental molar heat capacity of the two complexes with the reduction temperature (x) using the least-square method. ($x = [T - (T_{\max} + T_{\min})/2]/[T_{\max} - T_{\min})/2]$ [33], T_{\max} is the upper limit temperature (423.15 K), and T_{\min} is the lower limit temperature (278.15 K).

Complex 1 [Eu(2-FBA)₃(5,5'-DM-2,2'-bipy)]₂ T = (278.15–423.15) K.

$$C_{p,m}/\text{J}\cdot\text{K}^{-1}\cdot\text{mol}^{-1} = 1457.31206 + 296.09243x - 9.85364x^2 + 6.27545x^3.$$

$$R^2 = 0.99995 \text{ SD} = 1.32461.$$

Complex 2 [Tb(2-FBA)₃(5,5'-DM-2,2'-bipy)]₂ T = (278.15–423.15) K.

$$C_{p,m}/\text{J}\cdot\text{K}^{-1}\cdot\text{mol}^{-1} = 1486.32269 + 284.89958x - 8.80717x^2 + 14.6715x^3.$$

$$R^2 = 0.9999 \text{ SD} = 1.86495.$$

In the fitted polynomial equation, R^2 represents the correlation coefficient, and SD is the standard deviation of the fitted curves of the complexes. After that, using the fitted polynomial equation and the following thermodynamic equation, the smooth molar heat capacities and thermodynamic function of the complexes 1–2 with an interval

Fig. 6 FTIR spectra of the evolved gases for complexes 1 **a** and 2 **b**

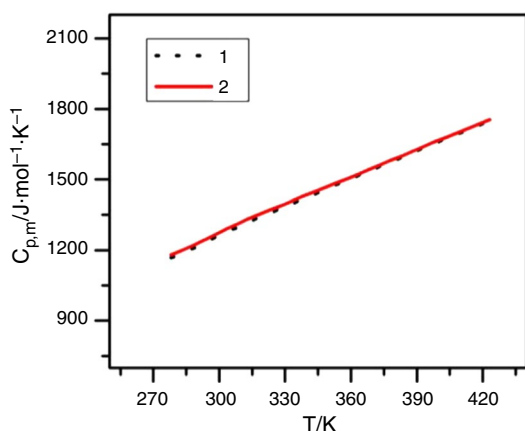
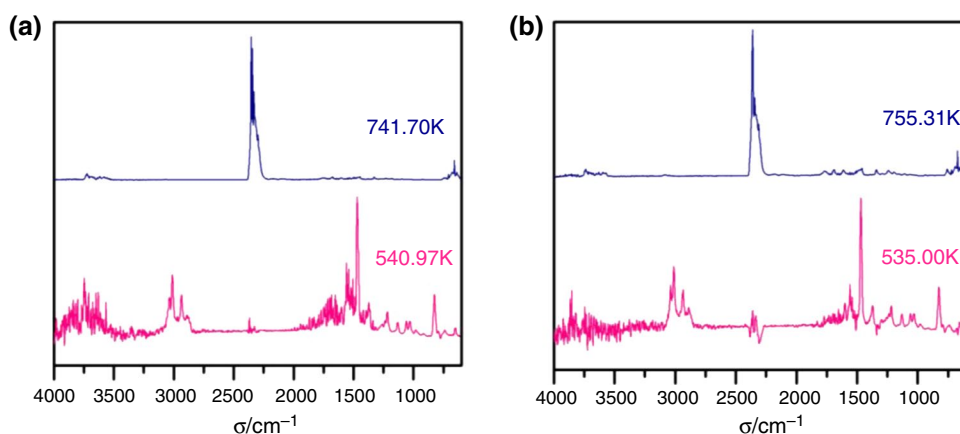


Fig. 7 Molar heat capacities of the complexes 1 and 2 varying with temperature (K) measured by DSC

of 5 K are calculated [34]. (298.15 K as standard reference temperature)

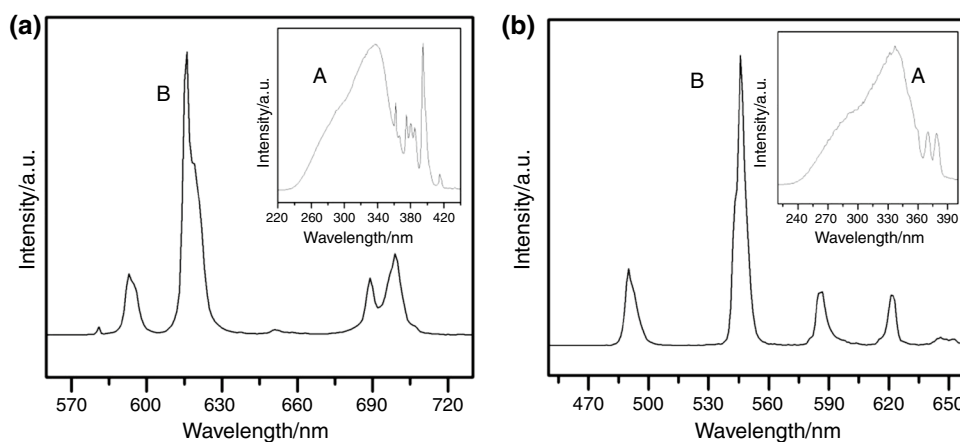
$$H_T - H_{298.15} = \int_{298.15}^T C_{p,m} dT$$

$$S_T - S_{298.15} = \int_{298.15}^T C_{p,m} T^{-1} dT$$

Excitation and emission spectra

The solid-state fluorescence spectra of complexes 1 and 2 are measured on the crystalline samples at room temperature, and the results are shown in Fig. 8a, b. The broad emission bands of both complexes are located in the range of 240–360 nm. As for complex 1, upon excitation at 337 nm, the impressive characteristic Eu(III) emissions are obtained in the visible region. Besides, there are a few weak excitation peaks in the range of 360–420 nm, which are created by the transition of f-f configuration of Eu(III). These results indicate that 2-FBA ligand can sensitize the emission of Eu(III). As described in Fig. 8a, all expected characteristic emission

Fig. 8 Solid-state emission and excitation spectra of complexes 1 **a** and 2 **b**



peaks of Eu(III) complex are observed: the corresponding electronic transitions: ${}^5D_0 \rightarrow {}^7F_0$ (581 nm), ${}^5D_0 \rightarrow {}^7F_1$ (593 nm), ${}^5D_0 \rightarrow {}^7F_2$ (615 nm), ${}^5D_0 \rightarrow {}^7F_3$ (651 nm), ${}^5D_0 \rightarrow {}^7F_4$ (699 nm) [35]. The emission intensity of 615 nm (${}^5D_0 \rightarrow {}^7F_2$) is higher than others, so complex 1 emits red light [36]. And it is obvious that the emission intensity at 593 and 615 nm is stronger, which is caused by the ${}^5D_0 \rightarrow {}^7F_1$ and ${}^5D_0 \rightarrow {}^7F_2$ transitions, respectively. The former is magnetic dipole, which is not sensitive to the coordination environment, while the latter is electric dipole, whose strength increases with the decrease in the symmetry of the site. The spectra of Eu(III) complex show that the former is weaker than the latter, indicating that Eu(III) is located in the low symmetry position without inversion center [37].

Figure 8b shows that the maximum excitation wavelength of complex 2 is 332 nm, the maximum emission value is 546 nm, and the monitoring range is 230–400 nm. Tb(III) complex exhibits four characteristic peaks at 490 nm, 546 nm, 587 nm and 621 nm, and the corresponding transition is ${}^5D_4 \rightarrow {}^7F_1$ ($J=6-3$) [38]. Obviously, ${}^5D_4 \rightarrow {}^7F_5$ at 546 nm occupies almost the entire emission spectrum, giving the most intense green luminescence output for Tb(III) complex.

Fluorescence lifetime

Moreover, the fluorescence lifetime of lanthanide complexes is of great significance. In order to gain fluorescence lifetime, fluorescence decay curves of complexes 1 and 2 are surveyed at room temperature. The attenuation curves and fitting curves for the two complexes are shown in Fig. 9. And the fluorescence decay curves of the complexes are fitted to the double exponential decay law, which satisfies the equation: $I(t) = B_1 \cdot \exp(-t/\tau_1) + B_2 \cdot \exp(-t/\tau_2)$ [39]. Where $I(t)$ represents the relative intensity, the decay time is τ_1 , τ_2 and B_1 , B_2 as constants. The fluorescence lifetime values of complexes 1 and 2 are calculated by using the equation $\tau = (B_1\tau_1^2 + B_2\tau_2^2)/(B_1\tau_1 + B_2\tau_2)$ [40]; their values are 1.471 ms and 0.609 ms, respectively.

In-depth luminescence studies have shown that both complexes have good fluorescence and the Eu(III) complex are better than that of Tb(III) complex, according to the experimental results of fluorescence lifetime, which indicates that aromatic carboxylic acids can sensitize Eu(III) ion of complex 1 more effectively. Therefore, the title complexes can be used for further research in the field of luminescent materials, and the former is better.

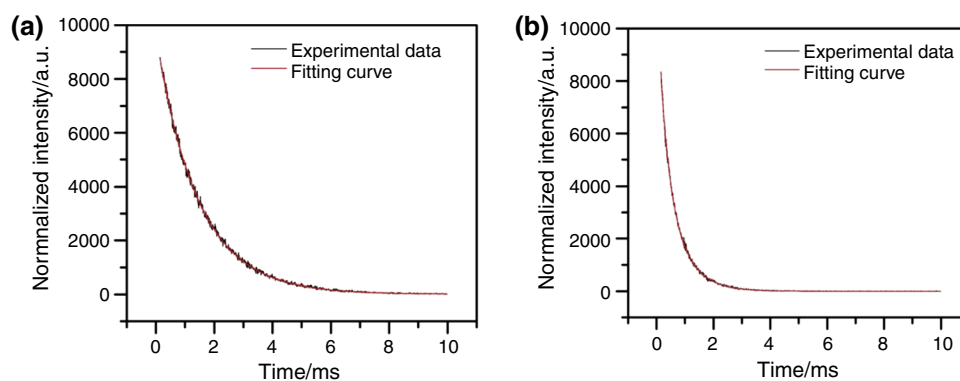
Conclusions

In summary, in the mixed solution of sodium hydroxide, water and 95% ethanol, lanthanide ions (Ln^{3+}) react with two ligands to obtain two nine-coordinated dinuclear complexes $[\text{Ln}(\text{2-FBA})_3(\text{5,5'-DM-2,2'-bipy})_2]$ [$\text{Ln} = \text{Eu}$ (1), Tb (2)]. Structural analysis indicates that both complexes are structurally analogous to each other. In addition, the binuclear molecules are further connected by hydrogen bonding to form one-dimensional and two-dimensional supramolecular structures, and their structures are comprehensively characterized by IR and TG-DSC/FTIR. The results show that the two complexes have high thermal stability. The molar heat capacities of the two complexes are investigated by a DSC instrument and their thermodynamic functions ($H_T - H_{298.15\text{K}}$) and ($S_T - S_{298.15\text{K}}$) are calculated. Furthermore, fluorescence studies show that the luminescence behavior of 1 and 2 is mainly from the characteristic emission of Eu(III) and Tb(III) centers, and their lifetimes are 1.471 ms and 0.609 ms, respectively. Based on the good fluorescence and thermal stability of complexes 1 and 2, they can be expected to have potential applications in the field of materials.

Supporting Information

The number of two complexes (CCDC 2019557 (1), CCDC 2019558 (2)) contains the supplementary crystallographic data for this paper. These data can be obtained free of charge from the Cambridge Crystallographic Date Centre via [www](http://www.ccdc.cam.ac.uk).

Fig. 9 **a** The lifetime decay curve of Eu(III) obtained by monitoring the emission at 615 nm; **b** the lifetime decay curve of Tb(III) obtained by monitoring the emission at 546 nm



ccdc.cam.ac.uk/data_request/cif. The experimental and smoothed molar heat capacities of complexes 1 and 2 are shown in Table S1, and thermodynamic functions of complexes 1 and 2 are shown in Table S2.

Acknowledgements The research work was supported by the National Natural Science Foundation of China (No. 21803016).

References

- Kovalenko A, Rublev PO, Tcelykh LO, Goloveshkin AS, Lepnev LS, Burlov AS, Vashchenko AA, Marciniak Ł, Magerramov AM, Shikhaliyev NG, Vatsadze SZ, Utochnikova VV. Lanthanide complexes with 2-(Tosylamino)-benzylidene-N-(aryloyl)hydrazones: universal luminescent materials. *Chem Mater*. 2019;31(3):759–73. <https://doi.org/10.1021/acs.chemmater.8b03675>.
- Ruiz C, García-Valdivia AA, Fernández B, Cepeda J, Oyarzabal I, Abas E, Laguna M, García JA, Fernández I, San Sebastian E, Rodríguez-Diéguez A. Multifunctional coordination compounds based on lanthanide ions and 5-bromonicotinic acid: magnetic, luminescence and anti-cancer properties. *Cryst Eng Comm*. 2019;21(25):3881–90. <https://doi.org/10.1039/c9ce00292h>.
- Wu ZL, Lan XW, Zhang YX, Li M, Bai GY. Copper(i) iodide cluster-based lanthanide organic frameworks: synthesis and application as efficient catalysts for carboxylative cyclization of propargyl alcohols with CO₂ under mild conditions. *Dalton Trans*. 2019;48(29):11063–9. <https://doi.org/10.1039/c9dt01859j>.
- Lyubov DM, Tolpygin AO, Trifonov AA. Rare-earth metal complexes as catalysts for ring-opening polymerization of cyclic esters. *Coord Chem Rev*. 2019;392:83–145. <https://doi.org/10.1016/j.ccr.2019.04.013>.
- Edelmann FT. Lanthanide amidinates and guanidinates: from laboratory curiosities to efficient homogeneous catalysts and precursors for rare-earth oxide thin films. *Chem Soc Rev*. 2009;38(8):2253–68. <https://doi.org/10.1039/b800100f>.
- Eliseeva SV, Bünzli JCG. Lanthanide luminescence for functional materials and bio-sciences. *Chem Soc Rev*. 2010;39(1):189–227. <https://doi.org/10.1039/b905604c>.
- Sabio RM, Santagneli SH, Gressier M, Caiut JMA, Pazin WM, Leite IS, Inada NM, Rosa da Silva R, Ribeiro SJL, Menu MJ. Luminescent nanohybrids based on silica and silylated Ru(II)-Yb(III) heterobinuclear complex: new tools for biological media analysis. *Nat Nanotechnol*. 2019;31(8):085709. <https://doi.org/10.1088/1361-6528/ab55c3>.
- Bünzli JCG. Lanthanide light for biology and medical diagnosis. *J Lumin*. 2016;170:866–78. <https://doi.org/10.1016/j.jlumin.2015.07.033>.
- Wu FS, Yang LL, Yue LX, Wang K, Liu GY, Luo XG, Zhu XJ. Ln(III) chelates-functionalized carbon quantum dots: synthesis, optical studies and multimodal bioimaging applications. *Colloids Surf B Biointerfaces*. 2019;175:272–80. <https://doi.org/10.1016/j.colsurfb.2018.11.054>.
- Xu DZ, Liu MY, Huang Q, Chen JY, Huang HY, Deng FG, Wen YQ, Tian JW, Zhang XY, Wei Y. One-step synthesis of europium complexes containing polyamino acids through ring-opening polymerization and their potential for biological imaging applications. *Talanta*. 2018;188:1–6. <https://doi.org/10.1016/j.talanta.2018.05.003>.
- Rossin A, Giambastiani G, Peruzzini M, Sessoli R. Amine-templated polymeric lanthanide formates: synthesis, characterization, and applications in luminescence and magnetism. *Inorg Chem*. 2012;51(12):6962–8. <https://doi.org/10.1021/ic300854b>.
- Gao BJ, Qiao ZW, Chen T. Structure and photoluminescence property of complexes of aromatic carboxylic acid-functionalized polysulfone with Eu(III) and Tb(III). *Mater Chem Phys*. 2014;143(3):1119–30. <https://doi.org/10.1016/j.matchemphys.2013.11.012>.
- Yan B. Recent progress in photofunctional lanthanide hybrid materials. *RSC Adv*. 2012;2(25):9304–24. <https://doi.org/10.1039/c2ra20976d>.
- Chen FF, Chen ZQ, Bian ZQ, Huang CH. Sensitized luminescence from lanthanides in d–f bimetallic complexes. *Coord Chem Rev*. 2010;254(9–10):991–1010. <https://doi.org/10.1016/j.ccr.2009.12.028>.
- Mara D, Artizzu F, Laforce B, Vincze L, Van Hecke K, Van Deun R, Kaczmarek AM. Novel tetrakis lanthanide β-diketonate complexes: structural study, luminescence properties and temperature sensing. *J Lumin*. 2019;213:343–55. <https://doi.org/10.1016/j.jlumin.2019.05.035>.
- Xu LJ, Xu GT, Chen ZN. Recent advances in lanthanide luminescence with metal-organic chromophores as sensitizers. *Coord Chem Rev*. 2014;273–274:47–62. <https://doi.org/10.1016/j.ccr.2013.11.021>.
- Gai YL, Jiang FL, Chen L, Wu MY, Su KZ, Pan J, Wan XY, Hong MC. Europium and terbium coordination polymers assembled from hexacarboxylate ligands: structures and luminescent properties. *Cryst Growth Des*. 2014;14(3):1010–7. <https://doi.org/10.1021/cg401452p>.
- Feng R, Jiang FL, Wu MY, Chen L, Yan CF, Hong MC. Structures and photoluminescent properties of the lanthanide coordination complexes with hydroxyquinoline carboxylate ligands. *Cryst Growth Des*. 2010;10(5):2306–13. <https://doi.org/10.1021/cg100026d>.
- ManjuBala Kumar S, Chahar S, Taxak VB, Boora P, Khatkar SP. Synthesis, NMR and optical features of intense green color terbium(III) complexes. *Optik*. 2020;202:163636. <https://doi.org/10.1016/j.ijleo.2019.163636>.
- Ren N, Wang F, Zhang JJ, Zheng XF. Progress in thermal analysis kinetics. *Acta Phys-Chim Sin*. 2020;36(6):1905062. <https://doi.org/10.3866/PKU.WHXB201905062>.
- Wang JJ, Zhang JJ. Thermal analysis kinetics and thermokinetics. *Acta Phys-Chim Sin*. 2020;36(6):1909020. <https://doi.org/10.3866/PKU.WHXB201909020>.
- Qiao CF, Lü L, Xu WF, Xia ZQ, Zhou CS, Chen SP, Gao SL. Synthesis, thermal decomposition kinetics and detonation performance of a three-dimensional solvent-free energetic Ag(I)-MOF. *Acta Phys-Chim Sin*. 2020;36(6):1905085. <https://doi.org/10.3866/PKU.WHXB201905085>.
- Wu XH, Ren N, Zhang JJ, Wang DQ. Lanthanide complexes with 2-bromo-5-methoxybenzoic acid and 5,5'-dimethyl-2,2'-bipyridine: crystal structures, thermodynamic properties and luminescence behaviors. *J Chem Thermodyn*. 2018;123:99–106. <https://doi.org/10.1016/j.jct.2018.04.002>.
- Sologubov SS, Markin AV, Sarmini YA, Samosudova YS, Smirnova NN, Boldyrev KL, Tatarinova EA, Meshkov IB, Muzafarov AM. Calorimetric study of siloxane dendrimer of the third generation with trimethylsilyl terminal groups. *J Therm Anal Calorim*. 2019;138(5):3301–10. <https://doi.org/10.1007/s10973-019-08693-9>.
- Pooley LI, Abu-Bakar AS, Cran MJ, Wadhvani R, Moinuddin KAM. Measurements of specific heat capacity of common building materials at elevated temperatures: a comparison of DSC and HAD. *J Therm Anal Calorim*. 2019;141(4):1279–89. <https://doi.org/10.1007/s10973-019-09124-5>.
- Fang DW, Gong L, Fan XT, Liang KH, Ma XX, Wei J. Low-temperature heat capacity and standard thermodynamic functions of the novel ionic liquid 1-(2-methoxyethyl)-3-ethyl imidazolium

- perrhenate. *J Therm Anal Calorim.* 2019;138(2):1437–42. <https://doi.org/10.1007/s10973-019-08295-5>.
27. Marques LF, Cantaruti AAB, Correa CC, Lahoud MG, da Silva RR, Ribeiro SJL, Machado FC. First crystal structures of lanthanide-hydrocinnamate complexes: hydrothermal synthesis and photophysical studies. *J Photochem Photobiol A.* 2013;252:69–76. <https://doi.org/10.1016/j.jphotochem.2012.11.012>.
 28. Wang CY, Kang J, Zhang XQ, Zhao YL, Chu HB. Crystal structures and luminescence properties of lanthanide complexes with 4-bromobenzoate and nitrogen heterocyclic ligands. *J Lumin.* 2019;215:116638. <https://doi.org/10.1016/j.jlumin.2019.116638>.
 29. Taha ZA, Ajlouni AM, Al Momani W, Al-Ghzawi AA. Syntheses, characterization, biological activities and photophysical properties of lanthanides complexes with a tetradentate schiff base ligand. *Spectrochim Acta A Mol Biomol Spectrosc.* 2011;81(1):570–7. <https://doi.org/10.1016/j.saa.2011.06.052>.
 30. Shi J, Hou YJ, Chu WY, Shi XH, Gu HQ, Wang BL, Sun ZZ. Crystal structure and highly luminescent properties studies of bis-beta-diketonate lanthanide complexes. *Inorg Chem.* 2013;52(9):5013–22. <https://doi.org/10.1021/ic302726z>.
 31. Zhu MM, Ren N, Zhang JJ, Wang DQ. Construction of three types of lanthanide complexes based on 3,4-dimethylbenzoic acid and 5,5'-dimethyl-2,2'-bipyridine: syntheses, structures, thermodynamic properties, luminescence, and bacteriostatic activities. *Appl Organomet Chem.* 2018;32(9):e4438. <https://doi.org/10.1002/aoc.4438>.
 32. Li YY, Ren N, He SM, Zhang JJ. Supramolecular structures, thermal decomposition mechanism and heat capacity of the novel binuclear Tb(III) and Dy(III) complexes with 2,3-dimethoxybenzoic acid and 5,5'-dimethyl-2,2'-bipyridine. *J Therm Anal Calorim.* 2019;140(5):2435–45. <https://doi.org/10.1007/s10973-019-08944-9>.
 33. Liu QS, Tan ZC, Welz-Biermann U, Liu XX. Molar heat capacity and thermodynamic properties of N-alkylpyridinium hexafluorophosphate salts, [C_npy][PF₆] (n=2, 3, 5). *J Chem Thermodyn.* 2014;68:82–9. <https://doi.org/10.1016/j.jct.2013.08.024>.
 34. He DH, Di YY, Wang B, Dan WY, Tan ZC. Low-temperature heat capacities and thermodynamic properties of ethylenediammonium tetrachlorozincate chloride (C₂H₁₀N₂)₂(ZnCl₄)Cl₂. *Thermochim Acta.* 2010;506(1–2):41–6. <https://doi.org/10.1016/j.tca.2010.04.012>.
 35. Kotyk CM, Weber JE, Hyre AS, McNeely J, Monteiro J, Domin M, Balaich GJ, Rheingold AL, de Bettencourt-Dias A, Doerr LH. Luminescence of lanthanide complexes with perfluorinated alkoxide ligands. *Inorg Chem.* 2020;59(14):9807–23. <https://doi.org/10.1021/acs.inorgchem.0c00782>.
 36. Zhou MX, Ren N, Zhang JJ. Crystal structure, thermal decomposition mechanism and properties of lanthanide supramolecular complexes based on 2,4,6-trimethylbenzoic acid and 5,5'-dimethyl-2,2'-bipyridine. *Acta Phys -Chim Sin.* 2021;37:2004071. <https://doi.org/10.3866/PKU.WHXB202004071>.
 37. Wang XQ, Zhang LL, Yang J, Liu FL, Dai FN, Wang RM, Sun DF. Lanthanide metal-organic frameworks containing a novel flexible ligand for luminescence sensing of small organic molecules and selective adsorption. *J Mater Chem A.* 2015;3(24):12777–85. <https://doi.org/10.1039/c5ta00061k>.
 38. Kukinov AA, Balashova TV, Ilichev VA, Trufanov AN, Ivin MN, Obolensky SV, Bochkarev MN. X-Ray excited luminescence of organo-lanthanide complexes. *Phys Chem Chem Phys.* 2019;21(29):16288–92. <https://doi.org/10.1039/c9cp03041g>.
 39. Sangeetha P, Jayaprakash P, Ramesh P, Sudha S, Vinitha G, Nageshwari M, Caroline ML. Crystal growth, spectroscopic, optical, thermal and hirshfeld surface analysis of glycinium hydrogen fumarate glycine solvate monohydrate (GHFGSM): a third harmonic nonlinear optical organic crystal. *J Mol Struct.* 2020;1213:128187. <https://doi.org/10.1016/j.molstruc.2020.128187>.
 40. Li HL, Liu YJ, Zheng R, Ma X, Chen LJ, Zhao JW. Syntheses, structures and fluorescence properties of three rare-earth containing dicosatungstates. *Spectrochim Acta A Mol Biomol Spectrosc.* 2017;176:114–22. <https://doi.org/10.1016/j.saa.2017.01.016>.

Publisher's Note Springer Nature remains neutral with regard to jurisdictional claims in published maps and institutional affiliations.